Petroleum Science 20 (2023) 2564–2574

Contents lists available at ScienceDirect

Petroleum Science

journal homepage: www.keaipublishing.com/en/journals/petroleum-science

Original Paper

Quantitatively probing interactions between membrane with adaptable wettability and oil phase in oil/water separation

Zhong-Zheng Xu [a, b], Ming-Wei Zhao [a, b, *], Yi-Ning Wu [a, b], Jia-Wei Liu [a, b], Ning Sun [a, b], Zi-Zhao Wang [a, b], Yi-Ming Zhang [a, b], Lin Li [a, b, **], Cai-Li Dai [a, b]

[a] Shandong Key Laboratory of Oilfield Chemistry, School of Petroleum Engineering, China University of Petroleum (East China), Qingdao, Shandong, 266580, China
[b] Key Laboratory of Unconventional Oil & Gas Development, China University of Petroleum (East China), Ministry of Education, Qingdao, Shandong, 266580, China

ARTICLE INFO

Article history:
Received 18 August 2022
Received in revised form
9 December 2022
Accepted 22 February 2023
Available online 24 February 2023

Edited by Jia-Jia Fei

Keywords:
Adaptable wettability
Selective oil/water separation
Interface interaction
Probe AFM technique

ABSTRACT

The membrane method based on adaptive wettability shows great advantages in oil-water separation. At present, researches focus on the excellent application performance of the membrane material, while the quantitative analysis of interactions in oil-water separation is rarely recognized. Herein, we constructed an adaptable wettability membrane with multiple polymer networks by polydopamine (PDA) and mussel-inspired amphiphilic polymer. Based on the Owens three-probe liquid method, the surface energy of the modified membrane was verified to meet the adaptive wettability conditions, with surface energies (γ_S) of 147.6 mJ m^{-2} (superhydrophilic/underwater superoleophobic) and 49.87 mJ m^{-2} (superhydrophobic/superoleophobic), respectively. The adhesion or repulsion of the membrane to the oil phase under different conditions during the separation process was quantified by the chemical probe AFM technique. In addition, the oil-water selective separation mechanism was further analyzed in a simplified membrane microchannel model. The results show that the different wetting produces capillary additional pressure in opposite directions, resulting in different energies to be overcome when the oil or water passes through the microchannels, thus achieving selective separation.

1. Introduction

With the development of interface science and bio-nanotechnology in recent years, special wettable materials have been developed by modulating the chemical functional groups and micro-nano roughness of solid surfaces (Ge et al., 2016; Lin et al., 2013; Zhu et al., 2013). The potential in oil-water separation applications is enormous. At present, according to their surface wetting properties, superhydrophilic/underwater superoleophobic materials with an “oil-removing” function and superhydrophobic/superoleophilic materials with a “water-removing” function have been developed (Wang and Chen, 2017; Wang et al., 2012). In addition, intelligent responsive separation materials have emerged that can reversibly change their surface wettability in response to external stimuli, and selective oil/water separation based on this property is achieved (Feng et al., 2004; Wang et al., 2007). Adaptable wettability is a unique stimulus-responsive material that does not require any continuous external stimuli (*e.g.*, pH (Li et al., 2016), light (Caputo et al., 2009), temperature (Lei et al., 2017), etc.). Materials with adaptable wettability require only simple pre-wetting to enable reversible switching between underwater superoleophobic (water pre-wetting) and underoil superhydrophobic (oil pre-wetting). Our group (Li et al., 2020) prepared a mussel-inspired membrane with adaptable wettability for oil/water separation, in which the polymer network was constructed on the surface of a stainless-steel membrane by crosslinking polydopamine with a synthetic amphiphilic polymer to each other. The polymer network exhibits amphiphilicity in the air. When pre-

* Corresponding author. Shandong Key Laboratory of Oilfield Chemistry, School of Petroleum Engineering, China University of Petroleum (East China), Qingdao, Shandong, 266580, China.
** Corresponding author. Shandong Key Laboratory of Oilfield Chemistry, School of Petroleum Engineering, China University of Petroleum (East China), Qingdao, Shandong, 266580, China.
E-mail addresses: zhaomingwei@upc.edu.cn (M.-W. Zhao), lilin@upc.edu.cn (L. Li).

https://doi.org/10.1016/j.petsci.2023.02.025

wetted by water, the polymer network is filled with water to form a hydrogel layer, exhibiting superhydrophilic/underwater superoleophobic. When pre-wetted by oil, the polymer network is filled with oil to form an organic gel film, exhibiting superhydrophobic/superoleophilic.

Special wettability mainly refers to the extreme wetting of a solid surface (Zhu and Guo, 2016). In general, if only the influence of surface chemical functional groups is considered, liquids tend to wet on solid surfaces with higher surface tension. When the surface tension of a solid is lower than that of a liquid, a lyophobic surface can be formed. Additionally, the roughness of the solid surface can promote and amplify the wettability of the solid surface, making droplet contact angles greater than 150° to reach super-lyophobic (Lin, 2005). At present, the methods for the construction of special wettable surfaces have been well established, materials with special wettability are prepared by spraying (Baldelli et al., 2020; Qiu et al., 2021), etching (Lian et al., 2018; Lu et al., 2020; Togonal et al., 2014), electrostatic spinning (Shami et al., 2019; Yan et al., 2021), sol-gel (Yabu et al., 2020; Zhu et al., 2020), self-assembly (Dai et al., 2020; Gao et al., 2011; Van et al., 2013), etc. are emerging. All types of membranes are modified to show special wettability, which is the key to achieving selective oil/water separation. Essentially the modification process results in a change in the surface energy of the membrane. However, most previous reports only describe the special wettability of surfaces by macroscopic contact angle measurements in different air or liquid environments, there are few studies on the change of surface energy before and after modification. Apart from the above, the current researches on oil-water separation membrane methods have focused on the hydrophilic or oleophilic properties resulting from physical/chemical modifications of the surface. The selective removal of oil or water is described only by differences in surface wettability. However, current researches lack quantitative analysis of the interaction between the membrane and the liquid throughout the oil/water separation process, limiting the basic and deeper understanding of the oil/water selective removal by the membrane.

In recent years, atomic force microscopy (AFM) has been widely used to quantitatively measure the interactions between various substances (Xie et al., 2020). Different substances can be used as stylus tips by modification, such as molecular chains/chemical groups (Xie et al., 2017), colloidal particles (Liu et al., 2021), and liquid droplets/bubbles (Cui et al., 2017). Accordingly, through nano-force tests between the membrane and the contact liquid, new insights can be gained into the nature of the driving and blocking forces on the selective separation of oil and water through the membrane. The oil/water separation process involves a variety of interactions, including the interactions of modified layers on the membrane surface and capillary forces within the membrane pore channels. The developed AFM technique enables the simulation of the oil phase through the modification of oleophilic chains. Therefore, it allows the interaction of the modified membrane with the oil phase to be analyzed while avoiding the influence of capillary forces. The independent effects of hydrophilic/oleophilic forces on the modified layer and capillary forces within the membrane pore channel on oil/water separation have not been reported.

In this work, the special wettability of the modified membrane surface is analyzed from the perspective of the solid surface free energy. The interaction forces during the oil phase contact with the membrane surface are further analyzed by the AFM chemical force probe technique, to quantify the adhesion or repulsion between modified membrane and oil phase under different environmental conditions. The wetting difference and the transport behaviors between oil and water phases in the membrane channel are discussed and analyzed separately by the simplified model of the membrane microchannel.

2. Materials and methods

2.1. Materials

Glycerol and diiodomethane were used as probe liquids for solid surface free energy calculations, dodecyl mercaptan and ethanol were used for the modification of gold-plated probes. All the reagents were not further purified and were purchased from Aladdin Reagent Co., Ltd. All the aqueous solutions were prepared using deionized water. The stainless-steel membrane was purchased from Anping Shuangpeng Co., Ltd. Hebei, China.

As shown in Fig. 1, the pristine membrane was first immersed in the polydopamine solution to make the polydopamine uniformly modified on the membrane surface. The mussel-inspired polymer exhibited amphiphilic property (Li et al., 2020), containing hydrophilic chains, hydrophobic chains, and catechol adhesion groups. The amphiphilic polymer network would trap and bind the first contacted liquid inside, forming a thin and stable liquefied layer on the membrane surface. Thus, the adaptable wettability of the membrane was achieved.

2.2. Thermodynamic analysis of surface energy

2.2.1. Surface energy with special wettability

In general, the construction of a superhydrophilic or superoleophilic surface requires the solid surface tension to be similar to the liquid surface tension in contact, whereas a superhydrophobic or superoleophobic surface requires the solid surface tension to be less than a quarter of the solid surface tension (Tuteja et al., 2007). The modified membrane is superamphiphilic in air, whereas achieving selective separation requires opposite wettability to oil and water phases. Thus, the surface energy of the membranes in the oil/water separation process is discussed separately.

Due to the high surface tension of water, the solid surface has oleophilic/hydrophobic wetting characteristics, satisfying $\gamma_W > \gamma_S > \gamma_O$. Thus, the solid surface with special superoleophilic/superhydrophobic wettability can be constructed by adjusting the surface roughness appropriately. When the solid surface is superhydrophilic in air, the surface tension of the solid surface is greater than or similar to the surface tension of water ($\gamma_S > \gamma_W$). Thus, the solid surface must be superoleophilic in the air ($\gamma_S > \gamma_W > \gamma_O$). Accordingly, it is impossible for superhydrophilic and superoleophobic to exist on the same solid surface in air at the same time. However, in an aqueous environment, the extended Young's equation describes a liquid-liquid-solid three-phase contact angle. The three-way relationship between the contact angle of oil droplets on a solid surface and the surface tension of oil and water can be described by the Eq. (1) (Koltuniewicz et al., 1995; Quéré, 2008):

$$\cos\theta_{WO} = \frac{\gamma_O \cos\theta_O - \gamma_W \cos\theta_W}{\gamma_{OW}} \quad (1)$$

where γ is the surface tension, θ is the contact angle, and the subscript W and O represents water and oil, respectively. When the solid surface in air exhibits hydrophilic or superhydrophilic wetting properties, at this point, the conditions of $\gamma_S > \gamma_W > \gamma_O$, $0° > \theta_W > 90°$ and $0° > \theta_O > 90°$ exist. If the condition of $\gamma_O \cos\theta_O < \gamma_W \cos\theta_W$ is met, then, $\cos\theta_{WO} < 0$, $90° < \theta_{WO} < 180°$. In addition, combined with the amplification of the wetting properties by the surface roughness structure, the superhydrophilic/underwater superoleophobic surface is constructed.

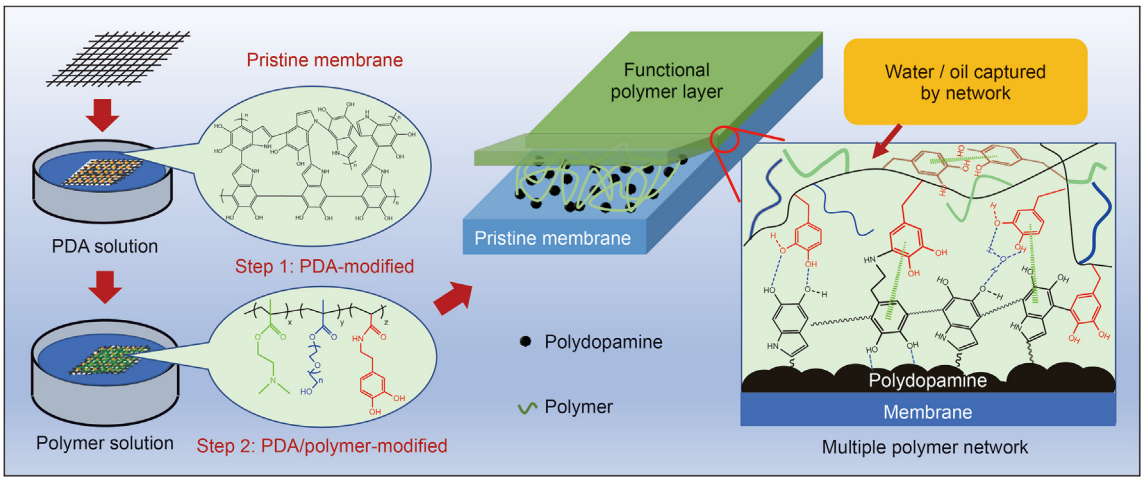

Fig. 1. Schematic description of the preparation of polymer/PDA-coated membrane.

2.2.2. Surface energy measurement

The surface energy of solids or liquids consists mainly of the Lifshitz-van der Waals (γ^{LW}) and the polar Lewis-acid/base (γ^{+}, γ^{-}). The surface energy of solid or liquid could be calculated from the G-Oss Eq. (2) (Oss, 2006):

$$\gamma = \gamma^{LW} + 2\sqrt{\gamma^{+}\gamma^{-}} \tag{2}$$

By relating G-Oss equation to the extended Young's formula (Wenzel, 1949; Young, 1832), the relationship between the free energy of interaction at the solid-liquid interface and the surface energy of solid and liquid can be obtained, as the following Eq. (3) (Owens and Wendt, 1969), where subscript S and L represent solid and liquid, respectively.

$$\cos\theta_L = \frac{\gamma_S - \gamma_{SL}}{\gamma_L} \tag{3}$$

$$\gamma_{SL} = \gamma_S + \gamma_L - 2\left(\sqrt{\gamma_S^{LW}\gamma_L^{LW}} + \sqrt{\gamma_S^{+}\gamma_L^{-}} + \sqrt{\gamma_L^{+}\gamma_S^{-}}\right) \tag{4}$$

The free energy of the solid-liquid interface (γ_{SL}) can be expressed as Eq. (4). Thus, the surface energy parameters of the solid can be calculated by combining Eqs. (3) and (4), provided that the contact angles of three liquids with known parameters are measured on the surface of the solid (Zhang et al., 2017). Distilled water, glycerol and diiodomethane are typical detection liquids for surface energy measurement by the three-liquid method. Their surface energy parameters are listed in Table 1.

2.3. Preparation of AFM chemical probe

The AFM chemical force probe technique is a special atomic force probe modification technique, in which molecular chains are modified on the tip surface by grafting, assembly and deposition (Hu et al., 2021). Consequently, the interaction forces between the modified molecular chains and a specific surface or substance can be measured with AFM. In this work, the probe type NPG-10 with a coefficient of elasticity of 0.24 N/m and resonance frequency of 56 kHz was used, and the tip of the needle is gold plated. The NPG-10 was immersed in a solution of dodecyl mercaptan/anhydrous ethanol at a concentration of 2.02 mg/mL, removed after 12 h and washed in anhydrous ethanol. Then dried using high-purity nitrogen. Dodecyl mercaptans form single molecule self-assembled films (SAMs) on the gold-plated tip by means of high bond strength S-Au bonds, with the alkyl chains spreading at a fixed angle in the direction normal to the gold surface (Shinn et al., 1999). The successful modification of dodecyl mercaptan was determined by SEM-EDS measurements of the tip surface elements.

Table 1
Surface energy parameters of the liquid used for detection.

Probing liquids	γ_L, mJ m^{-2}	γ_L^{LW}, mJ m^{-2}	γ_L^{+}, mJ m^{-2}	γ_L^{-}, mJ m^{-2}
Distilled water	72.8	21.8	25.5	25.5
Glycerol	64.0	34.0	3.92	57.4
Diiodomethane	50.8	50.8	0	0

2.4. Force measurement of oil in contact with membrane surface

As shown in Fig. 2, the gold-plated probe with modified straight chain alkanes was used as an oil phase to investigate the interaction between the oil phase and the membrane under different contact conditions (air, salinity, acidity, alkalinity). The AFM instrument type is MultiMode 8, from Bruker Co., Ltd. The force measurement mode used is Peak force QNM, with an approach or retract velocity of less than 0.2 μm/s throughout the force measurement process. The air or hydrodynamic perturbations can be ignored (Gao et al., 2018).

2.5. Mechanical analysis within simplified model of membrane microchannel

As shown in Fig. 3, the stainless-steel wire structure is simplified to a cylindrical skeleton of microchannels. The multiple network structure constructed by the PDA/polymer is simplified to a weak gel layer laid flat on the surface of the cylindrical skeleton. The diameter of the simplified microchannel model is approximated as the average pore size of the stainless-steel substrate membrane (3 μm). Due to the opposite wettability of the oil and water phases in relation to the modified membrane, both phases form different liquid surface shapes in the membrane microchannels. As a result, the direction and magnitude of the additional capillary pressure were different. The additional capillary pressure can be calculated from the Jurin Eq. (5) (Jiang et al., 2016; Yuan et al., 2020), where γ is the surface tension of a liquid, θ is the contact angle of the liquid on the membrane surface, R is the radius of microchannel.

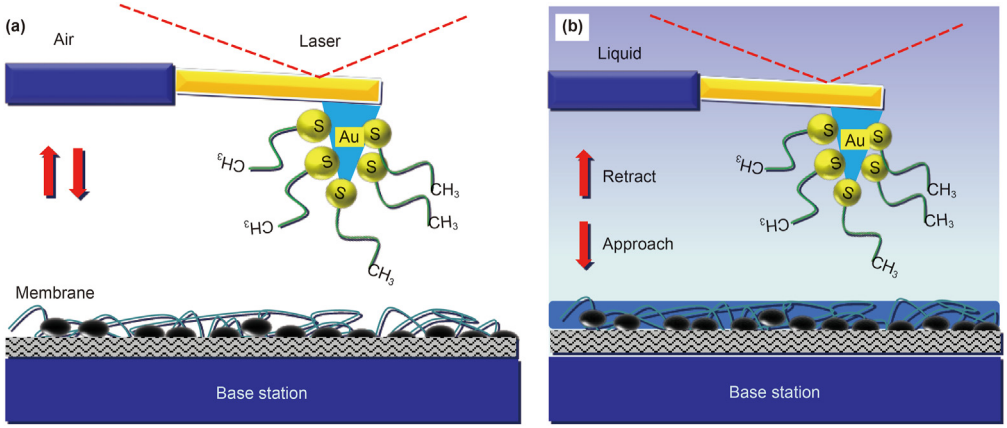

Fig. 2. Schematic diagram of force measurement of chemical-AFM: (**a**) air environment and (**b**) liquid environment.

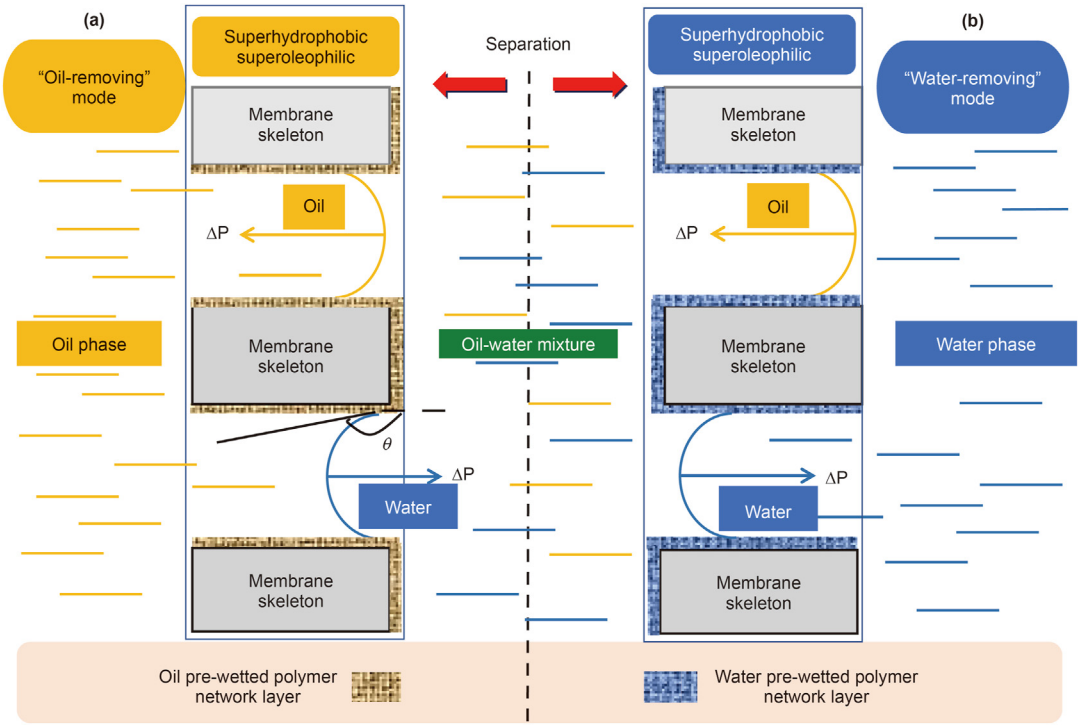

Fig. 3. Schematic of additional capillary pressure in simplified membrane channel: (**a**) "oil-removal" mode and (**b**) "water-removal" mode.

$$\Delta P = \frac{2\gamma \cos\theta}{R} \tag{5}$$

3. Results and discussion

3.1. Modification of PDA/polymer on membrane

The cross-knitted stainless steel metal membrane was selected as the substrate, which has strong mechanical strength and micron pores, and the average pore diameter is about 3 μm. Due to its high flux and low cost, it has been widely used in oil-water separation. Our group (Li et al., 2020) successfully prepared PDA/mussel-inspired amphiphilic polymer modified adaptive wettability metal membrane by two-step immersion method. The prepared modified membrane had excellent selective separation effect, with separation efficiency higher than 99.99% and separation rate up to 50 mL/min. Especially, after 15 cycles of separation test, the oil-water separation efficiency is still higher than 99.98%, proving that the modified membrane has excellent stability. The above excellent properties are mainly attributed to the rough structure of polydopamine and the functional properties of amphiphilic polymers. As shown in Fig. 4a, b, the pristine stainless steel membrane surface was clean and smooth, and the stainless-steel wire cross-knits constructed micron pores. Under the alkaline conditions provided by tris buffer solution, dopamine was easily oxidized to form polydopamine by intramolecular rearrangement and cross-linking after "Step 1" (Li et al., 2020). At this point, a large number of polydopamine nanoparticles with an average diameter of about 200 nm were observed on the membrane surface (Fig. 4c, d), which greatly increased the surface roughness. "Step 2" was used to

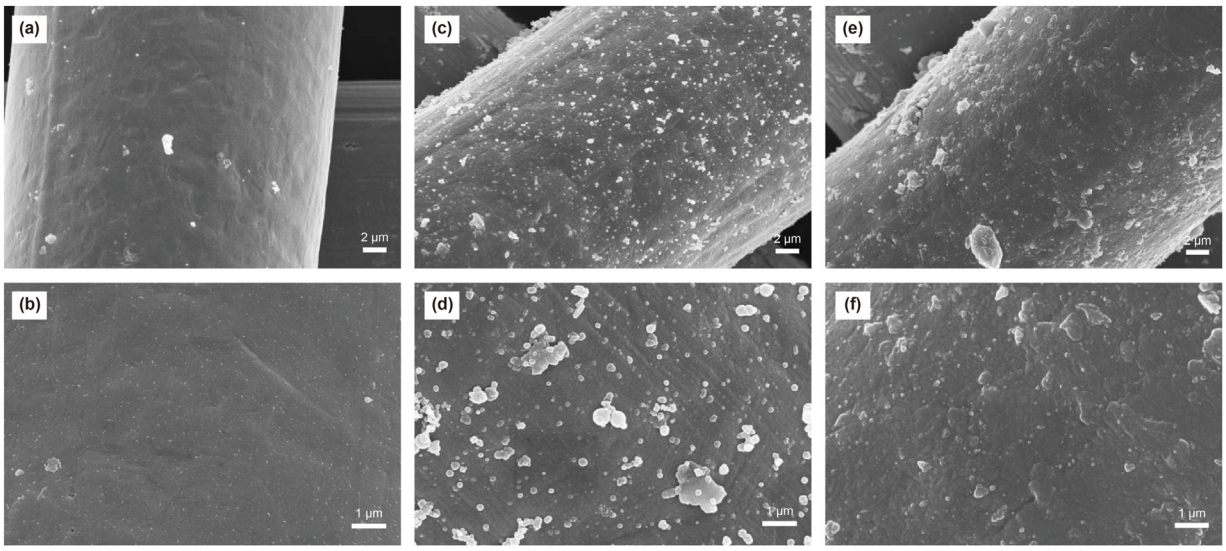

Fig. 4. SEM images of membranes at different processing stages: (**a**, **b**) pristine, (**c**, **d**) PDA-modified; (**e**, **f**) PDA/polymer-modified.

graft mussel-inspired amphiphilic polymer onto the PDA-coated membrane (Fig. 4e, f). By comparing Fig. 4c and d, it could be seen that the rough structure produced by PDA-coating was retained after the mussel-inspired amphiphilic polymer coating. The successful combination of surface roughness and functional polymer on the membrane surface was demonstrated.

The variation of surface roughness at different modification stages can be quantified by AFM with root mean square roughness (RMS). As shown in Fig. 5a, b, the RMS of the unmodified stainless-steel substrate was measured to be 15.9 nm. The RMS of the PDA-modified membrane and PDA/polymer-modified membrane were 22.8 nm and 28.6 nm, respectively, which was consistent with the SEM results. It was further proved that the modification of polymer does not lead to the disappearance of rough structure.

3.2. Surface energy of modified membrane

The surface energy conditions that should be available for the preparation of the modified membrane are as follows: ① When $\gamma_W > \gamma_S > \gamma_O$ is satisfied, the membrane can achieve super-hydrophobic/superoleophilic property. ② When $\gamma_S > \gamma_W > \gamma_O$ and $\gamma_O \cos\theta_O < \gamma_W \cos\theta_W$ are satisfied at the same time, the special wettability of the membrane with superhydrophilic/underwater superoleophobic property can be achieved. The surface energies of

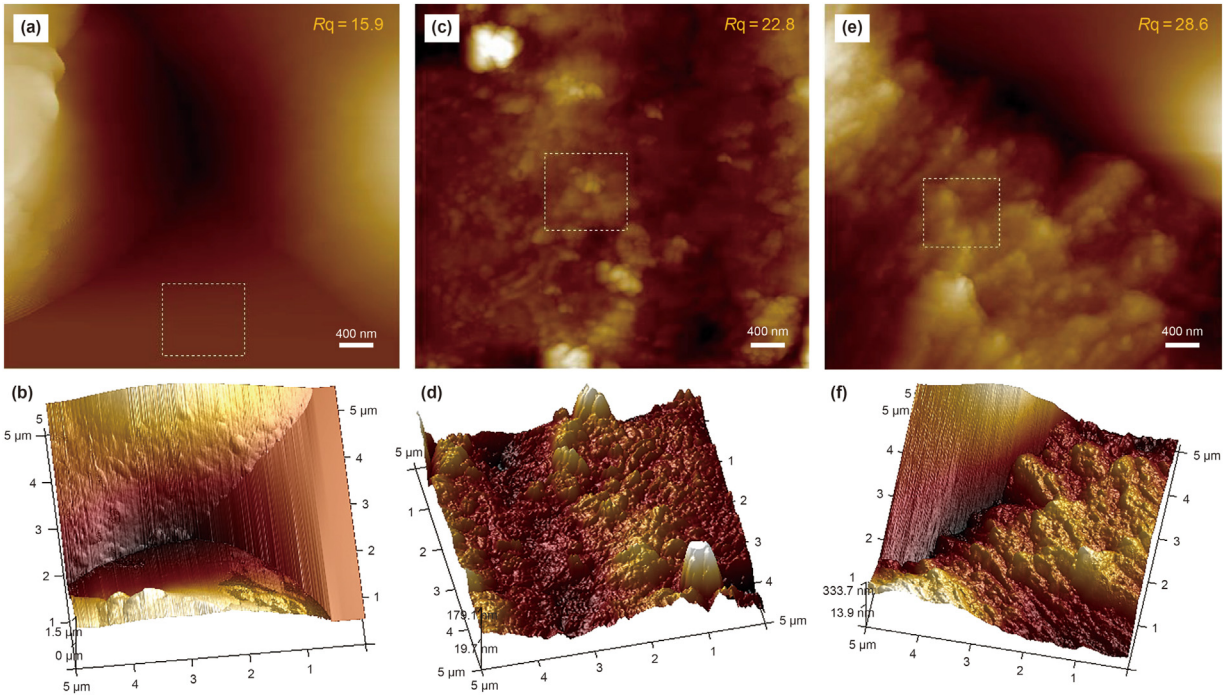

Fig. 5. AFM two-dimensional (2D) and three-dimensional (3D) images of membranes at different processing stages: (**a**, **b**) pristine, (**c**, **d**) PDA-modified, (**e**, **f**) PDA/polymer-modified. Dotted lines represent the specific position in the 2D image corresponding to the 3D image.

the modified membranes in different wetting states were determined by measuring the contact angles of purified water, glycerol and diiodomethane on the modified membranes. As shown in Table 2, the surface energies of the modified membrane with superhydrophilic/underwater superoleophobic and the modified membrane with superhydrophobic/superoleophilic were determined to be 147.6 mJ m^{-2} and 49.87 mJ m^{-2}, respectively. The results showed that the surface energy of the prepared modified membranes can meet both of these specific wettability conditions mentioned above. It was further demonstrated that the functional polymer and the micro-nano rough structure led to changes in the surface energy of the membrane.

3.3. Adhesion force measurement of oil contacting with membrane surface

3.3.1. Characterization of oleophilic AFM tip

As shown in Fig. 6 and Table 3, after modification by dodecyl mercaptan, the signal of Au element on the tip surface was weak, while S and C elements appeared in large numbers and uniformly on the probe surface, proving the successful modification of dodecyl mercaptan on the gold-plated probe surface. The relative atomic mass ratio of element C to element S was about 5.15, which was slightly higher than the ratio in dodecyl mercaptan (C:S = 4.5), indicating the successful modification.

Force mapping measurements of unmodified membrane and PDA/polymer modified membrane were carried out in air using a dodecyl mercaptan modified probe in a 500 nm range. As shown in Fig. 7, the microscopic morphology of the unmodified metal mesh substrate in air (Fig. 7a) showed flat and smooth. The distribution of adhesion force (Fig. 7b) and modulus (Fig. 7c) showed that the adhesion force of oil phase on the unmodified substrate ranges from 300 pN to 350 pN, and the modulus distribution was 8.9 MPa to 10.7 MPa, respectively, indicating that the surface of unmodified metal membrane was homogeneous and oleophilic.

Under the same conditions, the force measurements between the PDA/polymer modified membrane and oil phase were tested. In Fig. 7e, the adhesion force distribution increased to 0.5 nN~1.7 nN, indicating that the lipophilicity of the membrane surface was greatly enhanced after the modification. By comparing the adhesion force distribution plot with the surface microscopic morphology plot (Fig. 7d), it was found that the change in adhesion distribution coincided with the change in morphology due to surface modification. The modulus distribution (Fig. 7f) showed modulus of the raised portion was approximately 0.9 MPa, which was much lower than that of the unmodified membrane surface, further demonstrating that the substantial enhancement in oleophilic was due to the PDA/polymer modification on the membrane surface.

The measured adhesion histograms and fitted Gaussian distributions (solid curves) of the membrane before and after modification were shown in Fig. 8a and c, respectively. The fitted peak of the adhesion distribution on the pristine membrane surface showed a narrow single-peak distribution centered at 0.33 nN, indicating that the surface properties of the membrane were homogeneous before modification. After modification, the measured adhesion distribution was widened. But the fitted peak still showed a single peak distribution centered at 0.75 nN, demonstrating the enhanced oleophilic and the homogeneous modification of the PDA/polymer. Fig. 8b and d showed the force curves for a single point near the center of the fitted peak in Fig. 8a and c, respectively. The force-separation relationship between the oil phase and the unmodified membrane was shown in Fig. 8b, where only a weak attraction of approximately 320 pN was present throughout the force measured process, and the force applied over a relatively short range of approximately 25 nm. In Fig. 8d, the long-range attraction force appeared as soon as the tip approached the surface at approximately 27 nm. As the separation distance decreases, the attraction force first increased and then decreased. The repulsive force dominated at 12 nm, inferring that this may be due to an exponential increase in steric hindrance or electrostatic repulsion as the tip approached the surface. When the maximum load pressure was reached, the tip started to break away from the surface. Since the viscoelasticity and strong attraction of the PDA/polymer on the surface, the surface had a “pulling” effect on the oil phase to prevent it from leaving. The maximum adhesion force was calculated to be 0.75 nN for the entire force measurement process, much greater than the attraction of the membrane itself (320 pN) to the oil in the absence of polymer modification.

3.3.2. Force measurements in aqueous environment

In oil-water separation, oily wastewater inevitably exists in high salt and acidic environments, such as oilfield wastewater, industrial wastewater. Tapping Ramp force tests on the pristine membrane under different aqueous conditions (including water, 1 M NaCl and 1 M H_2SO_4, the conditions of the alkali environment were not considered as dodecyl mercaptan and alkali cannot co-exist) are shown in Fig. 9. The results of force measurements matched the force data in the air (Fig. 8b), the unmodified membrane under different aqueous solutions showed only a weak attraction to the oil phase. The adhesion forces in water, NaCl solution and H_2SO_4 solution were 0.80 nN, 0.15 nN and 0.30 nN, respectively. The results demonstrated the acceptable repeatability of the force measurements in the three solutions mentioned above.

The interactions of the modified membrane with the oil phase in the aqueous environment were discussed further, where the modified membrane could have contrasting wetting conditions of superoleophobic and superoleophilic through intelligent modulation (pre-wet by water or oil, respectively). As demonstrated in Fig. 10a, when the oleophilic tip gradually approached the membrane surface in a water environment, the entire force measurement process showed the repulsion between the oil phase and the membrane throughout, indicating that the modified membrane exhibited superhydrophilicity. Whereas in Fig. 10b, the long-range attraction force emerged at about 55 nm as the oleophilic tip contacted the modified membrane. The range of attraction provided by the PDA/polymer in a liquid environment was greater than its range of action in air (27 nm), with the resulting adhesion force increased to 3.86 nN. Meanwhile, a “jump out” phenomenon was evident during the tip retraction process. This was due to the fact that in the process of pulling up the probe, the attraction of the surface to the oil phase was broken as the driving force increased. At this point, the probe was suddenly released and bounced back to its initial position, thereby, some of the force data were lost. The

Table 2
Surface energy parameters of modified membranes.

Membranes	γ_S, mJ·m^{-2}	γ_S^{LW}, mJ·m^{-2}	γ_S^+, mJ·m^{-2}	γ_S^-, mJ·m^{-2}
Superhydrophilic/underwater superoleophobic	147.6	62.1	103.36	33.11
Superhydrophobic/superoleophili	49.87	45.64	0.12	37.28

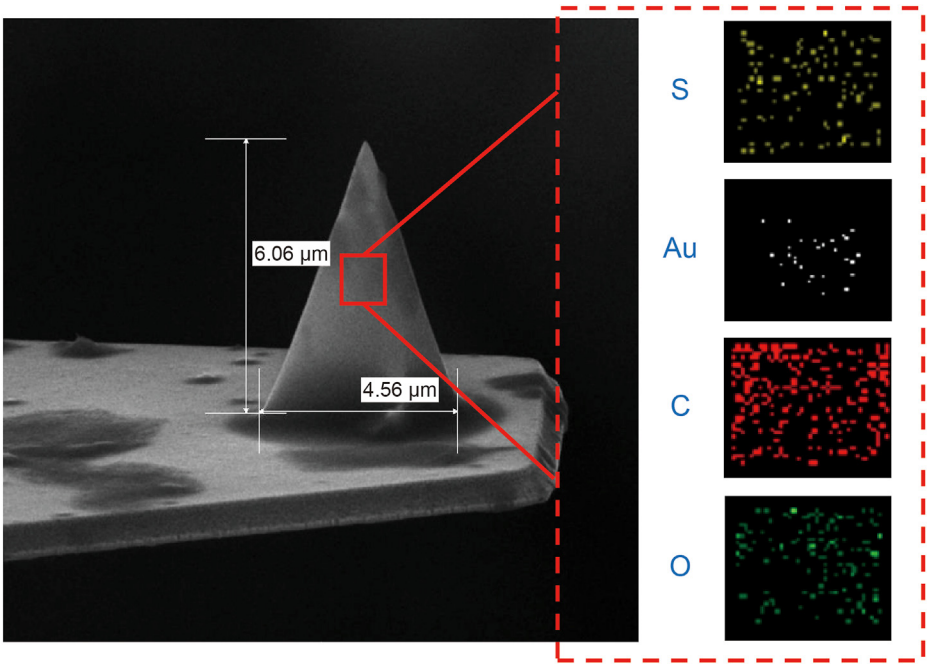

Fig. 6. SEM-EDS image of dodecyl coating probe force measurements in air environment.

Table 3
Element content of the dodecyl modified probe.

Element	C	S	O	Au
%	28.3	5.5	18.7	47.5

occurrence of the "jump out" phenomenon indicated that the interface had a significantly strong adhesion effect (Gao et al., 2018). The Young's modulus was calculated by fitting the force curve in Fig. 10b in Nanoscope software using the DMT model, with

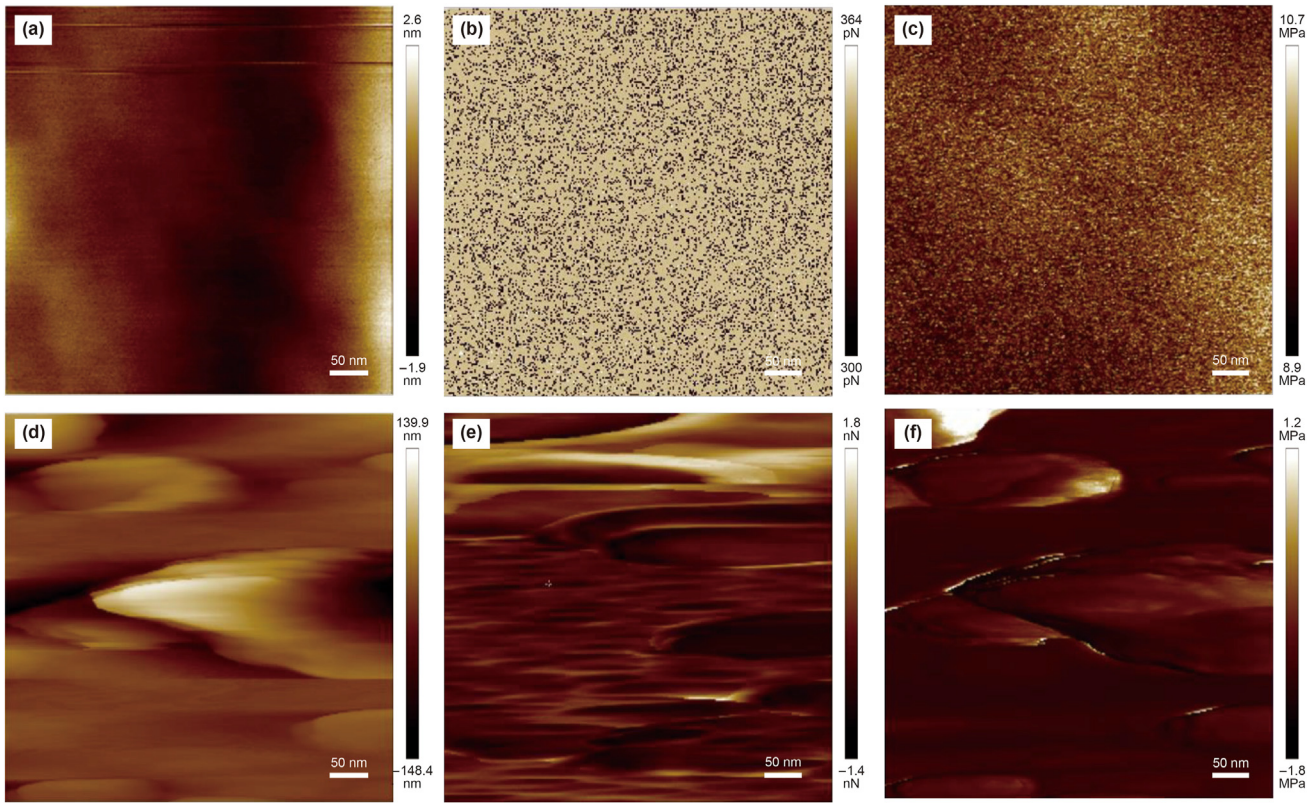

Fig. 7. Morphology (**a**), adhesive force (**b**) and modulus (**c**) of pristine membrane; morphology (**d**), adhesive force (**e**) and modulus (**f**) of modified membrane.

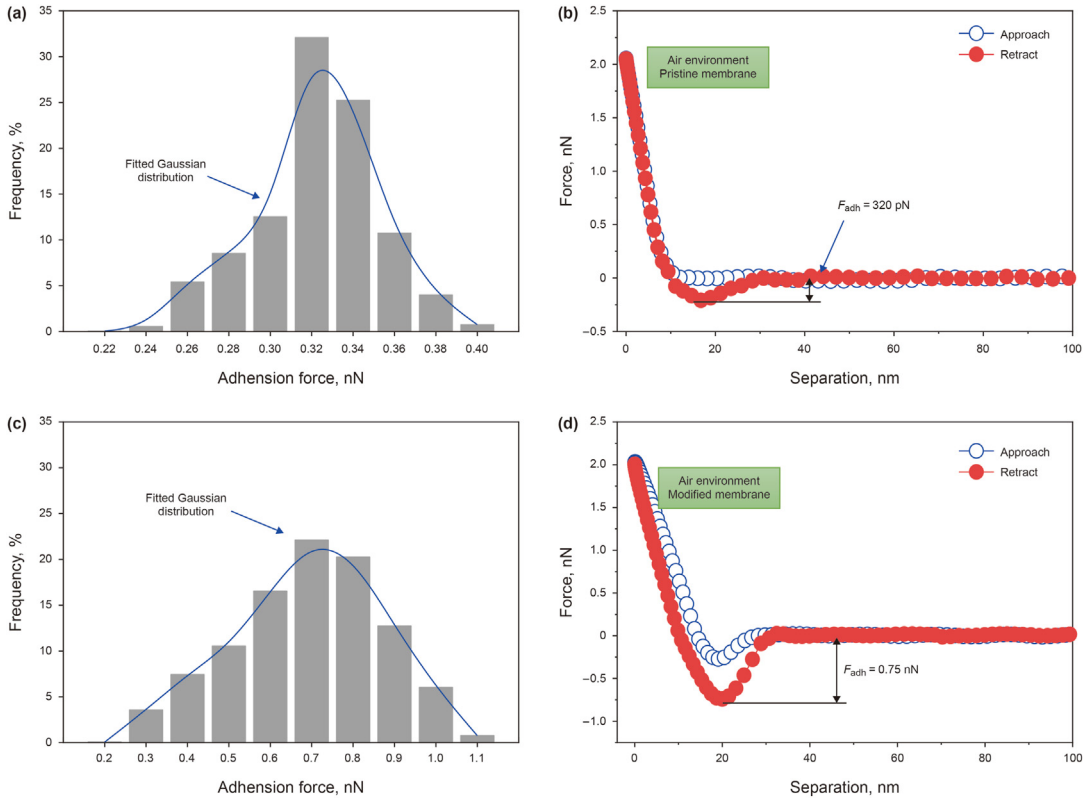

Fig. 8. Histograms of measured adhesion and force curves in air: (**a**, **b**) pristine membrane; (**c**, **d**) modified membrane.

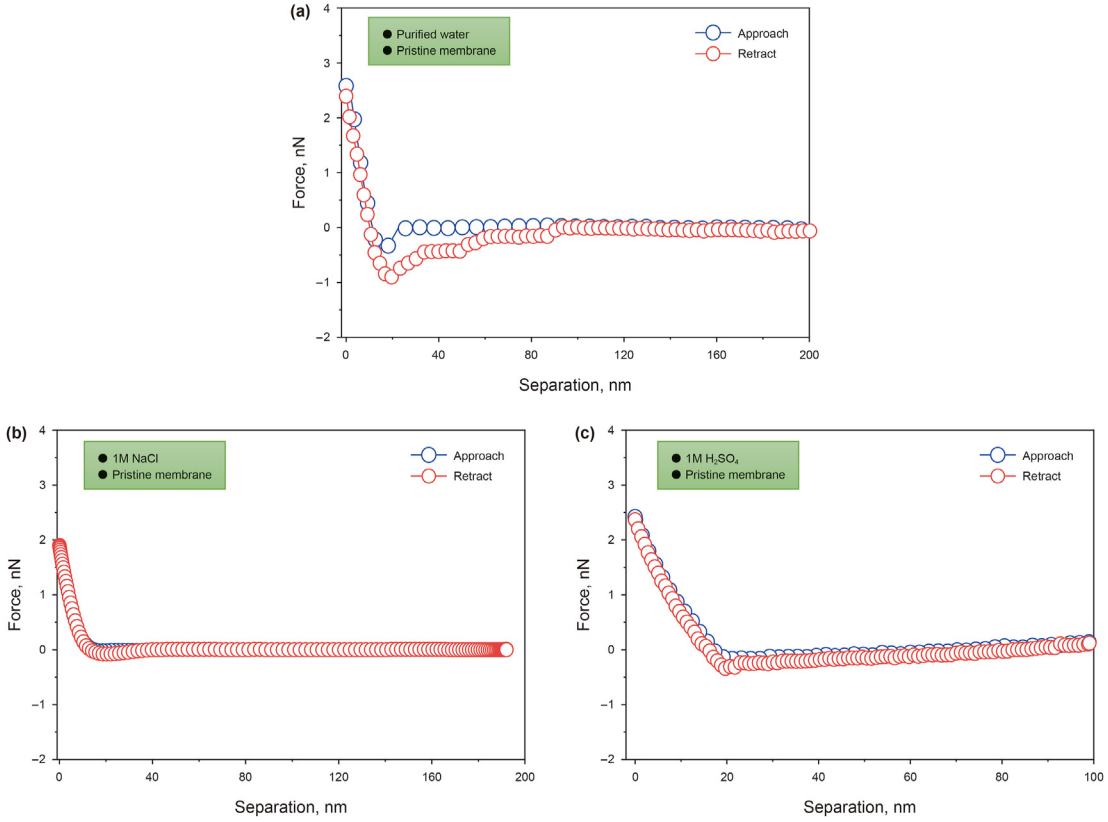

Fig. 9. Force curves of pristine membrane in different aqueous environment: (**a**) purified water; (**b**) 1 M Nacl; (**c**) 1 M H_2SO_4.

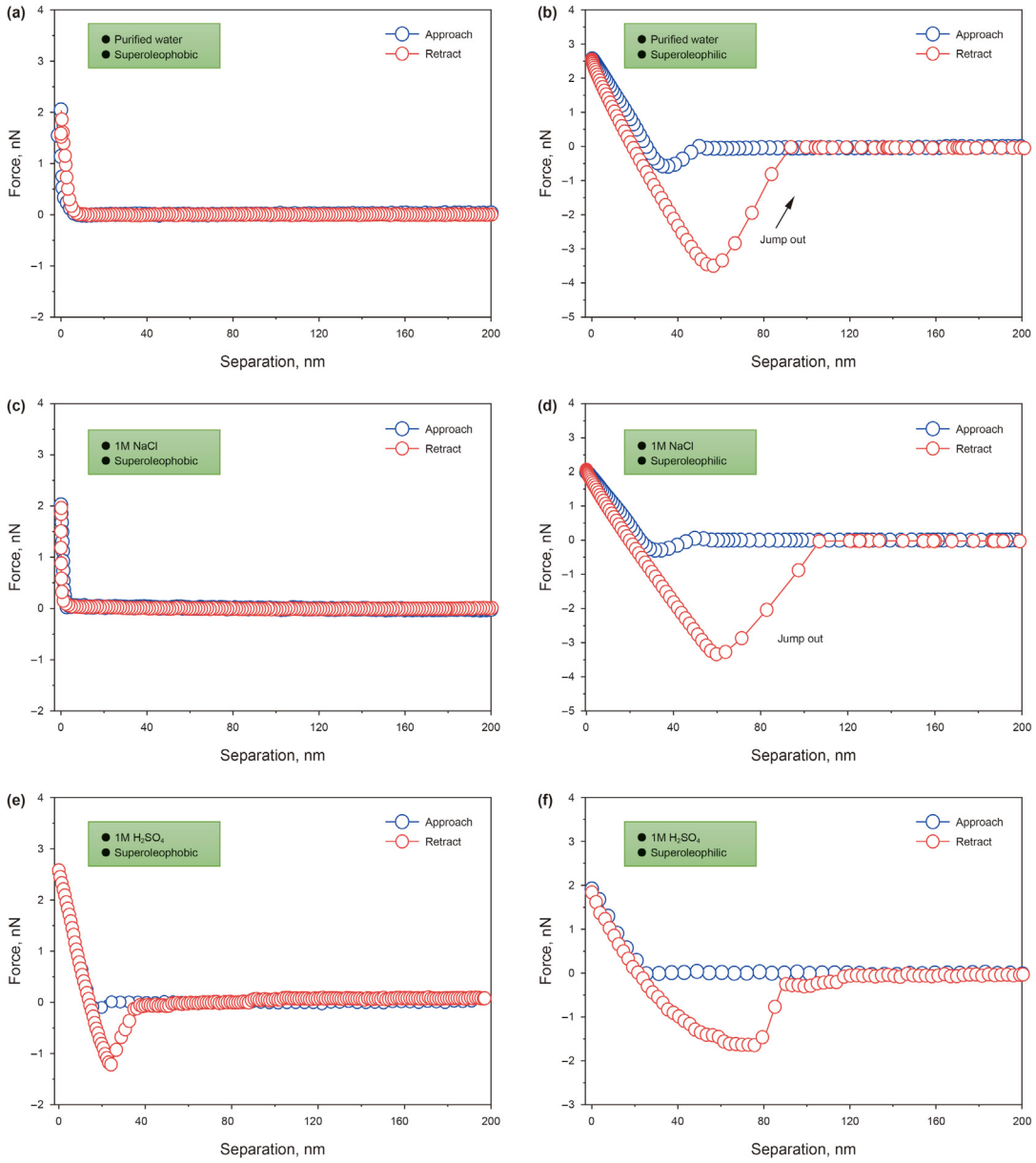

Fig. 10. Force curves of membranes with superoleophobic and superoleophilic in different aqueous environment: (**a**, **b**) purified water; (**c**, **d**) 1 M NaCl; (**e**, **f**) 1 M H_2SO_4.

the polymer network modulus reduced to ~0.2 MPa in liquid (approximately 0.9 MPa in air). The results demonstrated that the polymer layer can bind the first liquid contacted during the oil-water separation process, forming a weak gel layer on the membrane surface, and thus repelling other liquids (Xu et al., 2022).

To further determine the source of adhesion, force measurements were carried out under high salt conditions (1 M NaCl), where the high ionic concentration of the solution caused the compression of the diffused double layer, and therefore shielded the electrostatic forces (Lu et al., 2015). As shown in Fig. 10c, the full repulsion process between the oil phase and the hydrophilic membrane was still maintained. In Fig. 10d, the interaction between the oil phase and the hydrophilic membrane in the 1 M NaCl was similar to that in the purified water (Fig. 10a), with an attractive range of action of 46 nm and an adhesion force of 5.1 nN. This indicated that the salinity had little effect and the electrostatic forces were not predominant. Force measurements in 1 M H_2SO_4 solution were subsequently carried out. As shown in Fig. 10e, adhesion between the tip and the superoleophobic membrane was observed (approximately 1.2 nN). While the adhesion between the tip and the superoleophlilic membrane was decreased to 1.7 nN (Fig. 10f), presumably due to the reduced stability of the oil phase in an acidic environment.

3.4. Mechanism analysis within simplified model of membrane microchannel

The interaction between the oil phase and the PDA/polymer modified membrane was investigated by AFM chemical force probing techniques. It was demonstrated that due to the amphiphilicity of polymer, one phase of oil or water can be strongly attracted by the modified membrane while repelling another phase to prevent its contact with the separating membrane. When oil or water passed through the micropores of the membrane, capillary

Table 4
Calculation of additional capillary pressure for different separation modes.

Mixtures ΔP, kPa	Hexane/water		Dichloromethane/water		Toluene/water	
	Hexane	Water	Dichloromethane	Water	Toluene	Water
Water removal	−22.21	97.17	−28.98	97.17	−35.43	97.17
Oil removal	23.85	−90.63	30.8	−89.4	38.44	−89.57

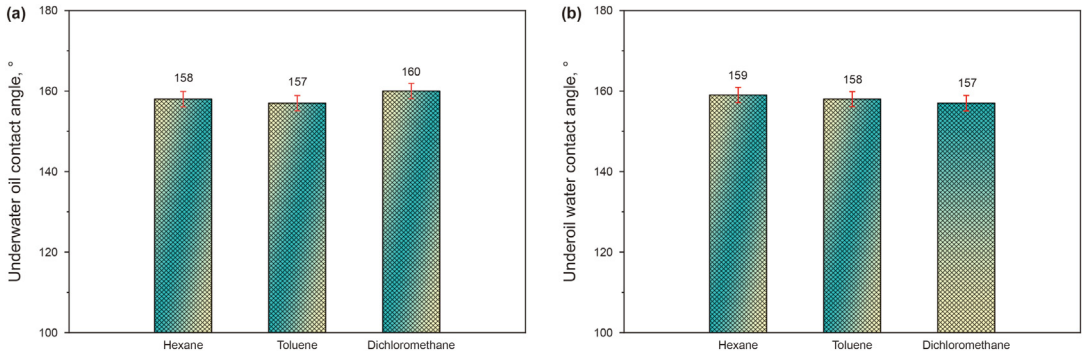

Fig. 11. Contact angle of polymer/PDA-coated membrane: (**a**) underwater oil contact angle; (**b**) underoil water contact angle.

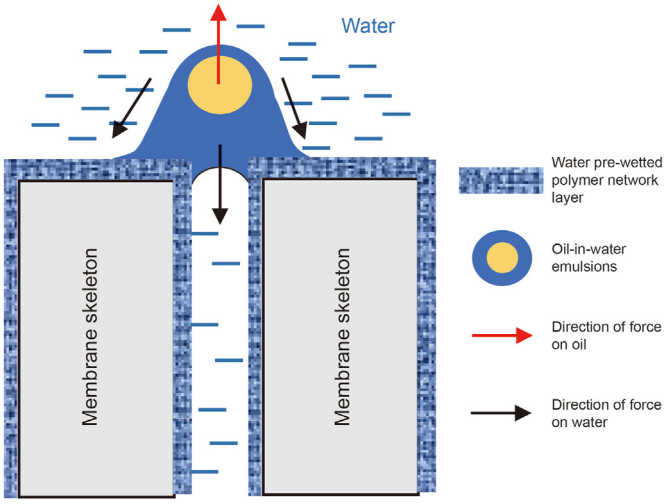

Fig. 12. Mechanism diagram of demulsification of simplified membrane microchannels.

forces should be essential to consider. Similarly, because of the opposite wettability of oil and water on the membrane, capillary forces were driving forces for one phase and the barrier for the other, as shown in Fig. 3. The additional capillary forces for different modes were calculated using Eq. (5), and the results were shown in Table 4, where positive values were the driving forces and negative values were the barrier forces (contact angles are shown in Fig. 11).

When the object of separation was an oil-water emulsion, as shown in Fig. 12, for the shell of the emulsion droplet, the capillary mechanic's additional pressure was the driving force during the separation process and simultaneously the multiple polymer network attracted the external phase. For the inner phase of the emulsion, in addition to the buoyancy or pressure caused by the difference in density between oil and water, there was a strong repulsive force preventing the oil droplets from approaching the membrane surface. For the whole droplet system, when the strength of all external forces (including the multiple attractions of the membrane to the outer shell and the strong repulsion of the membrane to the internal phase) were greater than the cohesive strength provided by the oil-water interface stabilized by the surface activator, demulsification was generated (Hlavacek, 1995; Zheng and Zhao, 1993).

4. Conclusions

In this work, the interactions between multi-polymer network modified membrane with special wettability and oil phase in the oil/water separation process were probed. The theoretical conditions for the specific wettability of membranes modified by a multi-polymer network were analyzed from a surface energy perspective as $\gamma_W > \gamma_S > \gamma_O$ or $\gamma_S > \gamma_W > \gamma_O$, $\gamma_O \cos\theta_O < \gamma_W \cos\theta_W$. The surface energy of the prepared modified membranes was verified to meet both conditions by surface free energy thermodynamic calculations (γ_S = 147.6 or 49.87 mJ m^{-2}). The interaction forces during the contact of the oil phase with the surface were analyzed by the AFM chemical force probe technique, quantifying the adhesion or repulsion of the membrane to the oil phase under different conditions. The mechanism of selective separation and demulsification was further elucidated by combining the mechanical analysis within a simplified model of membrane microchannels. The differential wetting produced capillary additional pressure in opposite directions, resulting in different energies to be overcome when the oil or water passes through the microchannels, thus achieving selective separation.

Declaration of competing interest

The authors declare no conflict of interest.

Acknowledgements

We gratefully acknowledge the financial support from National Key Research and Development Project, China (2019YFA0708700), the National Natural Science Foundation of China (52222403, 52074333) and the Innovation Fund Project for graduate students of China University of Petroleum (East China) (22CX04049A).

References

Baldelli, A., Ou, J.F., Li, W., Amirfazli, A., 2020. Spray-on nanocomposite coatings: wettability and conductivity. Langmuir 36 (39), 11393–11410. https://doi.org/10.1021/acs.langmuir.0c01020.

Caputo, G., Cortese, B., Nobile, C., et al., 2009. Reversibly light-switchable wettability of hybrid organic/inorganic surfaces with dual micro-/nanoscale roughness. Adv. Funct. Mater. 19 (8), 1149–1157. https://doi.org/10.1002/adfm.200800909.

Cui, X., Shi, C., Zhang, S., et al., 2017. Probing the effect of salinity and pH on surface interactions between air bubbles and hydrophobic solids: implications for colloidal assembly at air/water interfaces. Chem. Asian J. 12 (13), 1568–1577. https://doi.org/10.1002/asia.201700388.

Dai, C., Sun, W., Xu, Z., et al., 2020. Assembly of ultralight dual network graphene aerogel with applications for selective oil absorption. Langmuir 36 (45), 13698–13707. https://doi.org/10.1021/acs.langmuir.0c02664.

Feng, L., Zhang, Z., Mai, Z., et al., 2004. A super-hydrophobic and super-oleophilic coating mesh film for the separation of oil and water. Angew. Chem. Int. Ed. 43 (15), 2012–2014. https://doi.org/10.1002/anie.200353381.

Gao, Y.F., Huang, Y.J., Xu, S.Y., et al., 2011. Ordered honeycomb microporous films from self-assembly of alkylated guanosine derivatives. Langmuir 27 (6), 2958–2964. https://doi.org/10.1021/la1043969.

Gao, Z., Xie, L., Cui, X., et al., 2018. Probing anisotropic surface properties and surface forces of fluorite crystals. Langmuir 34 (7), 2511–2521. https://doi.org/10.1021/acs.langmuir.7b04165.

Ge, J., Zhao, H., Zhu, H., et al., 2016. Advanced sorbents for oil-spill cleanup: recent advances and future perspectives. Adv. Mater. 28 (47), 10459–10490. https://doi.org/10.1002/adma.201601812.

Hlavacek, M., 1995. Break-up of oil-in-water emulsions induced by permeation through a microfiltration membrane. J. Membr. Sci. 102, 1–7. https://doi.org/10.1016/0376-7388(94)00192-2.

Hu, Y., Chu, Z., Dai, C., et al., 2021. Probing of the hydrated cation bridges in the oil/brine/silica system via atomic force microscopy and molecular dynamics simulation. Fuel 306, 121666. https://doi.org/10.1016/j.fuel.2021.121666.

Jiang, J., Guo, Q., Wang, B., et al., 2016. Research on variation of static contact angle in incomplete wetting system and modeling method. Colloids Surf. A Physicochem. Eng. Asp. 504, 400–406. https://doi.org/10.1016/j.colsurfa.2016.05.051.

Koltuniewicz, A.B., Field, R.W., Arnot, T.C., 1995. Cross-flow and dead-end microfiltration of oily-water emulsion. Part I: experimental study and analysis of flux decline. J. Membr. Sci. 102, 193–207. https://doi.org/10.1016/0376-7388(94)00320-X.

Lin, F., 2005. Preparation and investigation of super-hydrophobic nanoscale interfacial materials. J. Grad. Sch. Chin. Acad. Sci. 22 (1), 106–109. https://doi.org/10.3969/j.issn.1002-1175.2005.01.017.

Lei, Z., Zhang, G., Deng, Y., et al., 2017. Thermoresponsive melamine sponges with switchable wettability by interface-initiated atom transfer radical polymerization for oil/water separation. ACS Appl. Mater. Interfaces 9 (10), 8967–8974. https://doi.org/10.1021/acsami.6b14565.

Li, J.J., Zhou, Y.N., Jiang, Z.D., et al., 2016. Electrospun fibrous mat with ph-switchable superwettability that can separate layered oil/water mixtures. Langmuir 32 (50), 13358–13366. https://doi.org/10.1021/acs.langmuir.6b03627.

Li, L., Xu, Z., Sun, W., et al., 2020. Bio-inspired membrane with adaptable wettability for smart oil/water separation. J. Membr. Sci. 598, 117661. https://doi.org/10.1016/j.memsci.2019.117661.

Lian, Z., Xu, J., Wang, Z., et al., 2018. Nanosecond laser-induced underwater superoleophobic and underoil superhydrophobic mesh for oil/water separation. Langmuir 34 (9), 2981–2988. https://doi.org/10.1021/acs.langmuir.7b03986.

Lin, N., Yang, H., Chang, Y., et al., 2013. Surface self-assembled pegylation of fluoro-based pvdf membranes via hydrophobic-driven copolymer anchoring for ultra-stable biofouling resistance. Langmuir 29 (32), 10183–10193. https://doi.org/10.1021/la401336y.

Liu, J., Li, L., Xu, Z., et al., 2021. Self-growing hydrogel particles with applications for reservoir control: growth behaviors and influencing factors. J. Phys. Chem. B 125 (34), 9870–9878. https://doi.org/10.1021/acs.jpcb.1c05289.

Lu, Y., Shen, Y., Tao, J., et al., 2020. Droplet directional movement on the homogeneously structured superhydrophobic surface with the gradient non-wettability. Langmuir 36 (4), 880–888. https://doi.org/10.1021/acs.langmuir.9b03411.

Lu, Z., Liu, Q., Xu, Z., et al., 2015. Probing anisotropic surface properties of molybdenite by direct force measurements. Langmuir 31 (42), 11409–11418. https://doi.org/10.1021/acs.langmuir.5b02678.

Oss, C., 2006. Interfacial forces in aqueous media, Second edition. Taylor and Francis, CRC Press.

Owens, D.K., Wendt, R.C., 1969. Estimation of the surface free energy of polymers. J. Appl. Polym. Sci. 13 (8), 1741–1747. https://doi.org/10.1002/app.1969.070130815.

Qiu, L., Kang, M., Guo, Z.G., et al., 2021. Simple method for the fabrication of multiple superwetting surfaces with photoresponse. Langmuir 37 (37), 11115–11122. https://doi.org/10.1021/acs.langmuir.1c01895.

Quéré, D., 2008. Wetting and roughness. Annu. Rev. Mater. Res. 38 (1), 71–99. https://doi.org/10.1146/annurev.matsci.38.060407.132434.

Shami, Z., Delbina, S., Amininasab, S.M., 2019. Wool-like fibrous nonwoven mesh with ethanol-triggered transition between antiwater and antioil superwetting states for immiscible and emulsified light oil-water separation. Langmuir 35 (32), 10491–10504. https://doi.org/10.1021/acs.langmuir.9b01032.

Shinn, N.D., Mayer, T.M., Michalske, T.A., 1999. Structure-dependent viscoelastic properties of C9>-alkanethiol monolayers. Tribol. Lett. 7 (2), 67–71. https://doi.org/10.1023/A:1019117319559.

Togonal, A.S., He, L.N., Cabarrocas, P.R.I., et al., 2014. Effect of wettability on the agglomeration of silicon nanowire arrays fabricated by metal-assisted chemical etching. Langmuir 30 (34), 10290–10298. https://doi.org/10.1021/la501768f.

Tuteja, A., Chol, W., Ma, M., et al., 2007. Designing superoleophobic surfaces. Science 318 (5856), 1618–1622. https://doi.org/10.1126/science.1148326.

Van, T.N., Lee, Y.K., Lee, J., et al., 2013. Tuning hydrophobicity of TiO2 layers with silanization and self-assembled nanopatterning. Langmuir 29 (9), 3054–3060. https://doi.org/10.1021/la304478s.

Wang, C.F., Chen, L.T., 2017. Preparation of superwetting porous materials for ultrafast separation of water-in-oil emulsions. Langmuir 33 (8), 1969–1973. https://doi.org/10.1021/acs.langmuir.6b04344.

Wang, C.F., Tzeng, F.S., Chen, H.G., et al., 2012. Ultraviolet-durable superhydrophobic zinc oxide-coated mesh films for surface and underwater-oil capture and transportation. Langmuir 28 (26), 10015–10019. https://doi.org/10.1021/la301839a.

Wang, Q., Cui, Z., Xiao, Y., et al., 2007. Stable highly hydrophobic and oleophilic meshes for oil-water separation. Appl. Surf. Sci. 253 (23), 9054–9060. https://doi.org/10.1016/j.apsusc.2007.05.030.

Wenzel, R.N., 1949. Surface roughness and contact angle. J. Phys. Colloid Chem. 53 (9), 1466–1467. https://doi.org/10.1021/j150474a015.

Xie, L., Cui, X., Gong, L., et al., 2020. Recent advances in the quantification and modulation of hydrophobic interactions for interfacial applications. Langmuir 36 (12), 2985–3003. https://doi.org/10.1021/acs.langmuir.9b03573.

Xie, L., Wang, J., Shi, C., et al., 2017. Mapping the nanoscale heterogeneity of surface hydrophobicity on the sphalerite mineral. J. Phys. Chem. C. 121 (10), 5620–5628. https://doi.org/10.1021/acs.jpcc.6b12909.

Xu, Z., Li, L., Liu, L., et al., 2022. Mussel-inspired superhydrophilic membrane constructed on a hydrophilic polymer network for highly efficient oil/water separation. J. Colloid Interface Sci. 608, 702–710. https://doi.org/10.1016/j.jcis.2021.09.123.

Yabu, H., Matsui, J., Matsuo, Y., 2020. Site-selective wettability control of honeycomb films by uv-o-3-assisted sol-gel coating. Langmuir 36 (40), 12023–12029. https://doi.org/10.1021/acs.langmuir.0c02401.

Yan, X., Xiao, X., Au, C., et al., 2021. Electrospinning nanofibers and nanomembranes for oil/water separation. J. Mater. Chem. 9 (38), 21659–21684. https://doi.org/10.1016/B978-0-323-51270-1.00013-3.

Young, T., 1832. An essay on the cohesion of fluids. Abstr. Pap. Print. Philos. Trans. R. Soc. Lond. 1, 171–172. https://doi.org/10.1098/rspl.1800.0095.

Yuan, T., Yin, J., Liu, Y., et al., 2020. Micro/nanoscale structured superhydrophilic and underwater superoleophobic hybrid-coated mesh for high-efficiency oil/water separation. Polymers 12 (6), 1378. https://doi.org/10.3390/polym12061378.

Zhang, C., Gong, L., Xiang, L., et al., 2017. Deposition and adhesion of polydopamine on the surfaces of varying wettability. ACS Appl. Mater. Interfaces 9 (36), 30943–30950. https://doi.org/10.1021/acsami.7b09774.

Zheng, Y.Y., Zhao, C.C., 1993. A study of kinetics on induced-air flotation for oil-water separation. Separ. Sci. Technol. 28 (5), 1233–1240. https://doi.org/10.1080/01496399308018032.

Zhu, H., Guo, Z., 2016. Understanding the separations of oil/water mixtures from immiscible to emulsions on super-wettable surfaces. JBE. 13 (1), 1–29. https://doi.org/10.1016/S1672-6529(14)60156-6.

Zhu, J., Jiang, J., Jamil, M., et al., 2020. Biomass-derived, water-induced self-recoverable composite aerogels with robust superwettability for water treatment. Langmuir 36 (37), 10960–10969. https://doi.org/10.1021/acs.langmuir.0c01690.

Zhu, Y., Zhang, F., Dong, W., et al., 2013. A novel zwitterionic polyelectrolyte grafted PVDF membrane for thoroughly separating oil from water with ultrahigh efficiency. J. Mater. Chem. 1 (18), 5758–5765. https://doi.org/10.1039/C3TA01598J.